Connections Matter: On the Importance of Pore Percolation for Nanoporous Supercapacitors

Oleg A. Vasilyev,[†,‡] Alexei A. Kornyshev,[*,¶] and Svyatoslav Kondrat[*,§]

†*Max-Planck-Institut für Intelligente Systeme, Heisenbergstraße 3, D-70569 Stuttgart, Germany*

‡*IV. Institut für Theoretische Physik, Universität Stuttgart, Pfaffenwaldring 57, D-70569 Stuttgart, Germany*

¶*Department of Chemistry, Imperial College London, Molecular Sciences Research Hub, White City Campus, London W12 0BZ, United Kingdom*

§*Department of Complex Systems, Institute of Physical Chemistry, PAS, Kasprzaka 44/52, 01-224 Warsaw, Poland*

E-mail: a.kornyshev@imperial.ac.uk; svyatoslav.kondrat@gmail.com;skondrat@ichf.edu.pl

Abstract

Nanoporous supercapacitors play a key role in energy storage and thereby attract growing interest of the research community. Development of porous electrodes for supercapacitors is of the paramount importance, but their characterization still remains a challenge. Herein, we analyse two examples of the popular carbide-derived and activated carbon electrodes from the point of view of inter-pore connectivity and ion permeation. Due to limited percolation, the effective porosity, as seen by an ion, decreases with increasing the ion size, which can reduce the stored energy density substantially. Our results highlight the importance of high quality well-percolated porous electrodes for supercapacitors, and suggest that the inter-pore connectivity is

an important characteristic to consider when optimizing the existing and developing new electrode materials.

Electrical double layer capacitors, also called supercapacitors or ultracapacitors, store energy by a potential-driven adsorption of charge to counterbalance the electron charge of a porous electrode, known as double layer formation. As this process does not involve any chemical reaction, charge and discharge occur in minutes or seconds, and the lifetime of supercapacitors reaches more than 10^6 cycles (about 25 years), although the stored energy density remains moderate.[1] The highest achievable capacitance[2–4] and energy density[5] were obtained for supercapacitors with the average pore size matching the size of a desolvated ion. Extensive research effort was dedicated to developing such nanoporous electrodes, with controllable pore sizes and structure,[6–8] and understanding their charging characteristics.[9–13] Often activated carbons are used in supercapacitors, but carbide-derived carbons (CDCs) were shown to provide a narrower distribution of pore sizes;[6] the newly developed graphene[7] and MXene-based[8] electrodes appear to be promising candidates too, owing to their high specific surface areas and capacitances.

One of the key characteristics of a porous electrode is a pore size distribution (PSD). Typically, PSDs are extracted from the nitrogen or carbon dioxide adsorption isotherms via mapping the applied pressure onto the pore width.[14–17] However, other gases have also been used, for instance argon and hydrogen[14] as well as the water vapor.[18] The cases of equal and different PSDs obtained by different probes were reported;[16] the differences could be particularly due to inter-pore connectivity, which might appear different for different probes. Interestingly, the connectivity of pores was found to have a profound effect on the hysteresis of gas adsorption in mesopores,[19] which affects the determination of PSDs. Historically, pore connectivity was in the center of attention in 1950-1970s in the context of permeation of liquid electrolytes into various pore networks, in relation to transport phenomena in porous materials and macrokinetics in volume-feeling micro-porous electrodes.[20]

Herein, we study how inter-pore connectivity (pore percolation) influences the energy

storage in *nano*porous supercapacitors. To achieve this goal, we create model porous electrodes in a computer using the method of Gaussian random fields.[21,22] As an example, we take the parameters corresponding to CDC600 (titanium carbide-derived carbon at chlorination temperature 600°) and activated carbon (MSP20, Kansai Coke and Chemicals Co.); these parameters have been obtained by Prehal *et al.*[23,24] by matching the theoretical and experimental small angle X-ray scattering (SAXS) curves. To calculate the distribution of pore sizes, we use the geometric definition of Gelb and Gubbins[25] (Methods), which has the advantage over the adsorption-based techniques that it is independent of adsorption model and is free of regularization parameters.[17] We then perform Monte Carlo simulations of charging slit nanopores (Figure 1a), as described in Ref. 26 (see Methods). We obtain the stored energies for various pore widths and average them over the corresponding pore-size distributions, similarly as in Ref. 5. Here, however, we analyse explicitly the pore structure, to account for pore percolation effects, as detailed below.

Before describing the results of this analysis, it is important to discuss the role of ion size in the case of slit-shaped pores. Figure 1b shows the energy (per surface area) stored in a slit nanopore as a function of pore width for ions of different sizes, as obtained by Monte Carlo simulations (Methods). In line with the anomalous increase of capacitance in subnanometer pores,[2–4,10] the stored energy density also increases as the pores become narrower.[5] Interestingly, however, the smaller ions appear to be more beneficial for the energy storage in the case of narrow and wide pores (Figure 1b and d), and only in the intermediate regime the studied ions provide comparable energies (Figure 1c). A similar effect has been reported by Lee *et al.*,[27] who pointed out that the capacitance increases for decreasing ion size while keeping the ratio w/d constant (here w is the pore width and $d = d_{\pm}$ the ion diameter, assumed the same for cations and anions for simplicity). The increase is due to the lower entropic costs of packing smaller ions, and because of a stronger screening achieved by smaller ions at a fixed w/d;[10,27] these effects enhance the capacitance and hence the stored energy.[28] (It must be noted, however, that larger ions are normally

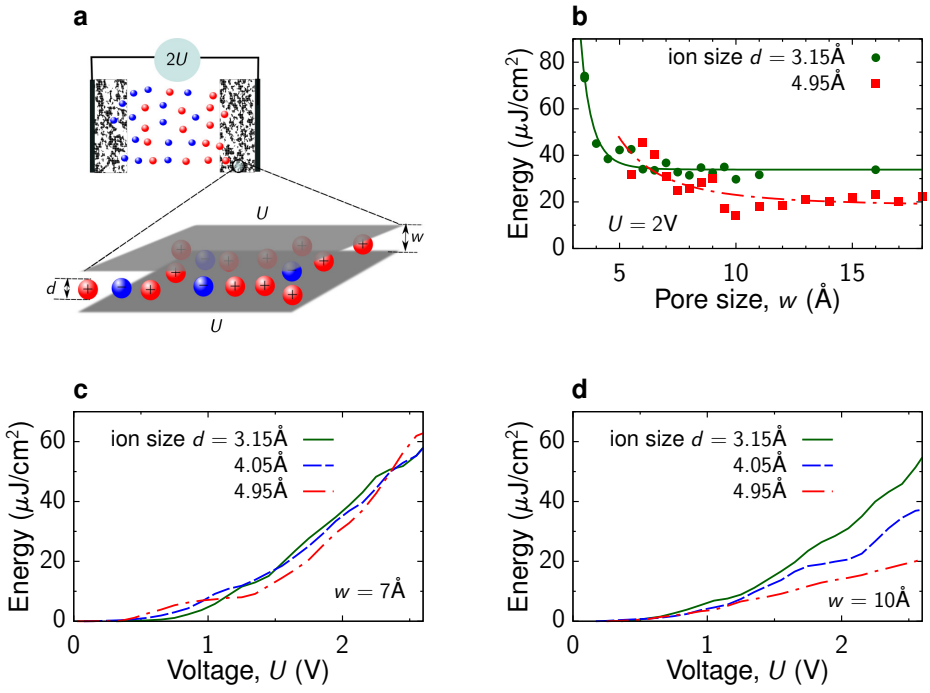

Figure 1: **Effect of ion size on the energy storage in slit nanopores.** (a) Schematics of a supercapacitor with nanoporous electrodes and of a model slit-shaped nanopore as a part of the supercapacitor's electrodes. The porous electrodes were generated by using the method of Gaussian random fields for titanium carbide-derived carbons chlorinated at 600 K (CDC600),[23] as described in Methods. (b) Energy per surface area stored in a slit nanopore as a function of pore width, w, for two ion diameters, d, at an applied potential $U = 2$V. Lines are a guide to the eye. (c-d) Energy stored in a slit nanopore as a function of applied voltage for a few ion diameters and for slit width $w = 7$Å (c) and $w = 10$Å (d).

associated with wider electrochemical windows, *i.e.*, the range of potentials above which they are reduced or oxidized at electrodes, allowing for higher applied voltages; proper ion-size optimization should take both effects into account.)

We now turn to nanoporous electrodes and describe the effect of inter-pore connectivity on the energy storage. To demonstrate its potential impact, we generated a *two-dimensional* CDC electrode and analyzed the accessibility of its pores to probes/ions of different sizes (we use 'probes' when discussing the properties of porous materials, such as connectivity and pore-size distributions, and 'ions' when discussing charging; clearly the geometric accessibility is the same for an ion and for a probe of the same size). In Figure 2, the carbon matrix is shown in black and the regions accessible to a probe in white; the region inaccessible to the

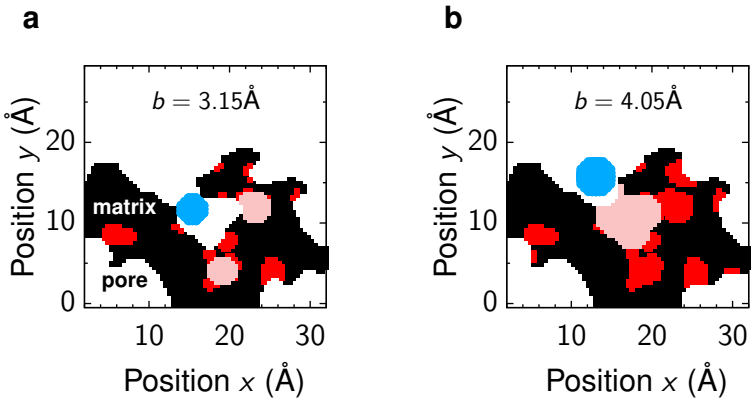

Figure 2: **Illustration of connectivity in porous materials.** For illustrative purposes, a porous structure was generated in two dimensions using the parameters of the CDC600 electrode. Carbon matrix is shown in black and the area accessible to the probes is left white. The pore area that is too narrow for the probes is shown in red; pink denotes the pore area that is sufficiently wide, but which is not accessible to the probes because it is connected to the main porous domain only by narrow isthmi, through which the probes cannot pass. Probe diameter $b = 3.15$ Å and $b = 4.05$ Å were used in (**a**) and (**b**), respectively.

probe consists of two subdomains coloured in pink and red. By red we denoted the porous region in which the probe could not fit, *i.e.*, such pores were too narrow; the pink marked the regions in which the probe *per se* could fit, but which were not accessible because they were connected to the main porous domain by narrow straits through which the probe could not pass. Figure 2b demonstrates that the number (surface area) of such 'disconnected' pores increases as the probe size increases.

To quantify the effect of pore percolation for real electrodes, we proceeded as follows. We first generated the CDC600 and MSP20 porous structures in a computer (Figure 3a,d, Methods). Then, we checked the connectivity of pores using the probes of different sizes, and eliminated those pores that were disconnected from the main porous domain, as seen by a given probe (*i.e.*, we turned the red and pink areas in Figure 2 into black; note that these areas depend on the probe size). For this *main* porous domain, we calculated the geometric PSDs by applying the method of Gelb and Gubbins[25] (Methods). Such PSDs for the CDC600 electrode and for two probes of different sizes are shown in Figure 3b. If the pores were all well-connected, independently of the probe size, then, clearly, all PSDs

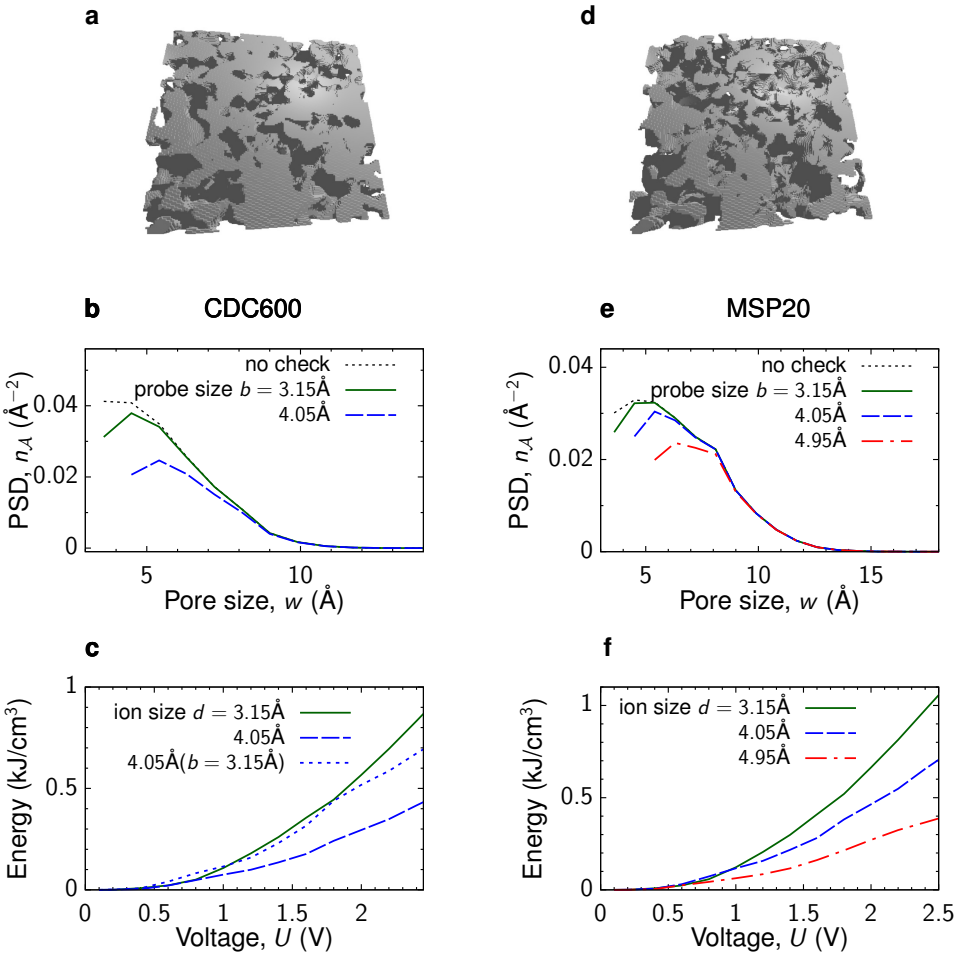

Figure 3: **Effect of pore percolation on the energy storage.** (**a**) Image of CDC600 porous electrode. (**b**) Effective pore size distributions (PSDs) of the CDC600 electrode obtained by probes of different diameter b. The effective PSD depends on the probe size because there are porous regions in the electrode that are connected to the main porous domain only by narrow straits, through which the probe cannot pass (see Figure 2). For comparison, the black dotted line shows the 'pristine' PSD, calculated without the connectivity check. (**c**) Energy density stored in the CDC600 electrode as a function of applied potential U for ions of different diameter d, which was obtained by averaging the Monte Carlo results (Figure 1) over the PSDs with the probe size $b = d$. For comparison, the blue dotted line shows the stored energy for ions of diameter $d = 4.05$ Å, averaged over the PSD obtained by the probe of diameter $b = 3.15$ Å $\neq d$. (**d**)-(**f**) The same as (a)-(c) but for the MSP20 activated carbon.

would coincide, except for pores of sizes $w < b$, where the probe of size b does not fit. However, Figure 3b shows that the PSDs coincide only for relatively wide pores, while there are notable deviations in the region of narrow pores, which are most significant for the

energy storage.[2–5,10] We have calculated the overall *probe-specific effective* porosity (*i.e.*, the porosity as seen by a particular probe) and obtained $\phi \approx 40\%$ and $\phi \approx 30\%$ for the probe sizes $b = 3.15\,\text{Å}$ and $b = 4.05\,\text{Å}$, respectively. Interestingly, the porosity, as seen by the 4.95 Å probe, turned out to be below 1% and is not shown in Figure 3b.

Clearly, the reduced effective porosity (the number of pores available) shall deteriorate the energy storage. To estimate its effect quantitatively, we averaged the stored energies obtained for slit pores (Figure 1) over the effective PSD with the probe size $b = d$, where $d = d_{\pm}$ is the ion diameter, assumed the same for cations and anions (eqn (5) in Methods). The result is shown in Figure 3c and demonstrates that the ion-specific pore percolation can have a substantial effect on the energy storage; in particular, the energy density is reduced nearly twice as the ion diameter increases from 3.15 Å to 4.05 Å. For comparison, in Figure 3c we also plot the energy density obtained for the 4.05 Å ion, but averaged over the PSD with the probe size 3.15 Å (blue dotted line in Figure 3c). Here, the difference with the $d = b$ case (solid green line) is only due to the ion-size effects (Figure 1), and the energy density follows the $d = b = 3.15\,\text{Å}$ curve more closely. This means that the main contribution to the reduction of the energy density is due to the reduced inter-pore connectivity for the ion of a given size. Figure 3d-f shows that such a percolation-induced reduction in PSDs and in stored energy densities persist also for the MSP20 activated carbon, and the magnitude of the effect is comparable to that of CDC600. (It is also interesting to note that the MSP20 electrode provides higher energy densities in all cases considered, which is due to the higher effective porosity as seen by all probes/ions. The most striking difference is for the 4.95 Å ion, for which the energy stored in the CDC600 electrode practically vanishes (data not shown), while it is essentially non-zero for the MSP20 (red dot-dash line in Figure 3f).)

For comparison, in Figure 3b,e we also show *pristine* PSDs, obtained without probing the inter-pore connectivity. Such PSDs correspond to hypothetical ideally-percolated porous electrodes, which thereby provide the highest energy storage capabilities, potentially achievable within a given structure (the corresponding energy densities depend on the ion size and

are not shown in Figure 3c,f for clarity of presentation). We note, however, that such electrodes are not optimal. An electrode, providing the highest possible energy density, likely consists of a stack of monodisperse slit pores with the slit-width optimized for given working voltage;[5] such an optimal electrode seems challenging to fabricate, however.

In conclusion, we have demonstrated that the ion size and pore percolation can have a vivid effect on the energy storage in nanoporous supercapacitors. It is important to note, however, that in our analysis of inter-pore connectivity, we assumed that the probes, ions and the particles of the pore matrix were hard spheres. This implies that the ion and the probe cannot fit into a pore smaller than their own size. In reality, the probes (ions) are 'soft' and seldom spherical and may fit into smaller pores, or pass through narrow straits between larger pores, *e.g.*, via their reorientation, at sufficiently high pressures (applied potentials). In addition, in our estimates the cations and anions were assumed to be of the same size, while in reality most ionic liquids are size asymmetric, implying asymmetry in pore-percolation by cations and anions, which may affect the energy storage. Further, to estimate the effect of percolation, we averaged the stored energies obtained for slit nanopores. A quick inspection of the generated porous structures (Figure 3a,d) suggests, however, that the pores are often not slit-shaped, but can be of any kind of shapes – cylindrical, spherical, 'triangular',[16] etc. It was shown that pore-size distributions are sensitive to the assumption of pore geometry,[29] and hence the so-averaged stored energies acquire an additional dependence on these assumptions.

It is clear that all these effects may influence the *quantitative* estimates provided in this work, and it will be interesting, and beneficial for supercapacitor optimization, to study them in greater detail. Nevertheless, our work clearly demonstrates the importance of good quality well-percolated nanoporous electrodes for maximizing the energy storage, and suggests that their detailed characterization, particularly for ion-specific porosity and inter-pore connectivity, can be crucial for the judicious design of an optimal supercapacitor.

Methods

Monte Carlo simulations

Grand canonical Monte Carlo simulations of charging slit nanopores, as in Figure 1a, have been performed by using a customized version of the Towhee simulation package (`http://towhee.sourceforge.net/`). The customization was needed to take into account the superionic state of ions in conducting nanoconfinement, which consists of the exponentially screened ion-ion interactions and of image-force attraction of ions to nanopore walls;[10] the details of the simulation method can be found in Ref. 26. In all simulations, temperature was $T = 298$ K, and we used a relative dielectric constant inside the pores $\varepsilon_r = 2.5$ to account for electronic degrees of freedom of ions (we assumed that ε_r is pore width independent, for the effect of pore-width dependent ε_r see Ref. 30). The resolvation energy, *i.e.*, the energy of transfer of ions from the bulk electrolyte into the pores, was $3.36k_BT$, and was chosen the same for cations and anions.

The system size was $50\,\text{Å} \times 50\,\text{Å} \times w$, where w is the slit width. The hard-core wall-ion interactions were supplemented by the image-force attraction of ions to the pore walls.[10] The ions were modeled as charged soft spheres using the standard Weeks-Chandler-Anderson repulsive-only potential[31] and the screened electrostatic potential in the superionic state for the charge-charge interactions.[10] The ion sizes were chosen to be a multiple of the lattice constant of the generated porous structures ($a = 0.045$nm, see below), in order to make a consistent analysis of the inter-pore connectivity and charging properties; the ion diameters were $d_\pm = 7a = 0.315$ nm, $d_\pm = 9a = 0.405$ nm, and $d_\pm = 11a = 0.495$ nm.

Monte Carlo steps included translational, Widom insertion/deletion[32] and molecular-type swap[26] moves. Each simulation consisted of 2×10^7 equilibration and 2×10^7 production moves.

Generation of nanoporous electrodes

We have used the method of Gaussian random fields[21,22] to generate the porous electrodes. In order to avoid hollow structures,[22] the electrodes were obtained by intersecting two statistically independent random fields (defined at each point $\boldsymbol{x}$ in space)

$$y_\nu(\boldsymbol{x}) = \sqrt{\frac{2}{N}} \sum_{i=1}^{N} \cos(\boldsymbol{k}_{\nu,i}\boldsymbol{x} - \varphi_{\nu,i}), \tag{1}$$

where $\nu = \{1, 2\}$, N is a number of wave-vectors used (we took $N = 500$ as in Ref. 23,24), $\varphi_{\nu,i} \in [0, 2\pi)$ is a uniformly distributed random variable, and the probability distribution of wave vectors $\boldsymbol{k}_{\nu,i}$ is[22]

$$P(k) = \frac{k\xi d}{\pi} \frac{\sinh(\pi k\xi/2)\sinh(\pi^2\xi/d)}{\cosh(\pi k\xi) + \cosh(2\pi^2\xi/d)}, \tag{2}$$

where ξ and d are two parameters characterizing the porous structure (see below). The porous matrix is determined by the set of all points $\boldsymbol{x}$ at which $y_\nu(\boldsymbol{x})$ simultaneously satisfy $\alpha \le y_\nu \le \beta$ ($\nu = 1, 2$). The parameters α and β are not independent, but are related to the porosity ϕ by $\phi = 1 - (p_\alpha - p_\beta)^2$, where ($A = \{\alpha, \beta\}$)[22]

$$p_A = \frac{1}{\sqrt{2\pi}} \int_{-\infty}^{A} \mathrm{e}^{-t^2/2} dt. \tag{3}$$

We generated the porous structures on a cubic lattice of size $10^3 \times 10^3 \times 10^3$ sites with the lattice constant $a = 0.045$nm. The parameters were $\xi = 0.26$nm, $d = 7$nm, $\alpha = -4$ ($\beta = 0.55$, intrinsic porosity $\phi = 0.50241$) for CDC600; and $\xi = 0.275$nm, $d = 7$nm, $\alpha = -4$ ($\beta = 0.3$, intrinsic porosity $\phi = 0.6$) for MSP20. These parameters have been obtained by Prehal *et al.*[23,24] by fitting the model to the small angle X-ray scattering curves obtained experimentally for the CDC600 and MSP20 electrodes. Within this approach, the main differences between the two carbons is the presence of wider pores and higher porosity of MSP20, as evidenced by the (effective) pore size distributions (PSDs, Figure 3b,e). It must

be noted here that the method of Gaussian random fields does not provide a unique porous structure, as it depends on the choice of the correlation function.[21,22] It would be beneficial to develop alternative (complementary) methods to reproduce porous structures more precisely, particularly those consisting of ultra-narrow pores.

Pore size distributions and averaging

To account for connectivity of pore space, we first removed all pores, in which a probe could not fit. Then, from the remaining pore space, we determined the largest porous domain and eliminated the pores that were not connected to it (because the connecting straits were too narrow for the probe to pass, Figure 2). To do this, we used the Hoshen-Kopelman algorithm for cluster labeling.[33] The pore size distribution (PSD) for this (main) porous domain was calculated by using the method of Gelb and Gubbins.[25] It is based on spanning the space available to the probe by a test particle of diameter w and determining the total volume $\Omega(w)$ spanned by this particle. Then the geometric PSD is, by definition,[25] $n_\Omega(w) = -d\Omega/dw$.

Assuming slit-shaped pores, as in many studies on pore size determination,[14–17] we obtained for the relevant pore size distribution function

$$n_{\mathcal{A}}(w) = -\frac{1}{wV_{el}}\frac{d\Omega}{dw}, \tag{4}$$

where V_{el} is the total volume of a porous sample (electrode). The function $n_{\mathcal{A}}(w)$, multiplied by V_{el}, gives the surface area of pores of width w; $n_{\mathcal{A}}$ is shown in Figure 3b,e. The energy per volume stored in an electrode is

$$\bar{E}_v(U) = \int_0^\infty E_s(U,w)n_{\mathcal{A}}(w)dw, \tag{5}$$

where $E_s(U,w)$ is the energy (per surface area) stored in a slit pore of width w at applied potential U; $\bar{E}_v(U)$ is shown in Figure 3c,f.

Acknowledgement

We are grateful to Christian Prehal and Volker Presser for sharing the parameters of the porous structures from Ref. 23,24. S.K. and A.K. acknowledge the CONIN project of the European Union's Horizon 2020 Research and Innovation Programme (Marie Skłodowska-Curie grant agreement no. 409 734276), and personally Alina Ciach (IPC, Warsaw) and Eva Noya (IPC Rocasolano, Madrid), for the invitation to CONIN Workshop in Madrid and interesting discussions. A.K. thanks Alexander von Humboldt foundation for support of his visit to Max-Planck Institute for Intelligent Systems (MPI-IS, Stuttgart). A.K. and S.K. are grateful to Professor Dietrich (MPI-IS) for hospitality and fruitful discussions. S.K. thanks Nikolaj Georgi for interesting debates on inter-pore connectivity.

References

(1) Miller, J. R.; Burke, A. F. Electrochemical Capacitors: Challenges and Opportunities for Real-World Applications. *Electrochem. Soc. Interface* **2008**, *17*, 53–57.

(2) Chmiola, J.; Yushin, G.; Gogotsi, Y.; Portet, C.; Simon, P.; Taberna, P. L. Anomalous Increase in Carbon Capacitance at Pore Sizes Less Than 1 Nanometer. *Science* **2006**, *313*, 1760–1763.

(3) Raymundo-Piñero, E.; Kierczek, K.; Machnikowski, J.; Béguin, F. Relationship Between the Nanoporous Texture of Activated Carbons and Their Capacitance Properties in Different Electrolytes. *Carbon* **2006**, *44*, 2498–2507.

(4) Largeot, C.; Portet, C.; Chmiola, J.; Taberna, P.-L.; Gogotsi, Y.; Simon, P. Relation Between the Ion Size and Pore Size for an Electric Double-Layer Capacitor. *J. Am. Chem. Soc.* **2008**, *130*, 2730–2731.

(5) Kondrat, S.; Pérez, C. R.; Presser, V.; Gogotsi, Y.; Kornyshev, A. A. Effect of Pore

Size and Its Dispersity on the Energy Storage in Nanoporous Supercapacitors. *Energy Environ. Sci.* **2012**, *5*, 6474–6479.

(6) Simon, P.; Gogotsi, Y. Materials for Electrochemical Capacitors. *Nat. Mater.* **2008**, *7*, 845–854.

(7) Chen, J.; Li, C.; Shi, G. Graphene Materials for Electrochemical Capacitors. *J. Phys. Chem. Lett.* **2013**, *4*, 1244–1253.

(8) Zhao, M.-Q.; Ren, C. E.; Ling, Z.; Lukatskaya, M. R.; Zhang, C.; Aken, K. L. V.; Barsoum, M. W.; Gogotsi, Y. Flexible MXene/Carbon Nanotube Composite Paper with High Volumetric Capacitance. *Advanced Materials* **2014**, *27*, 339–345.

(9) Feng, G.; Qiao, R.; Huang, J.; Sumpter, B. G.; Meunier, V. Ion Distribution in Electrified Micropores and Its Role in the Anomalous Enhancement of Capacitance. *ACS Nano* **2010**, *4*, 2382–2390.

(10) Kondrat, S.; Kornyshev, A. Superionic State in Double-Layer Capacitors with Nanoporous Electrodes. *J. Phys.: Condens. Matter* **2011**, *23*, 022201.

(11) Merlet, C.; Rotenberg, B.; Madden, P. A.; Taberna, P.-L.; Simon, P.; Gogotsi, Y.; Salanne, M. On the Molecular Origin of Supercapacitance in Nanoporous Carbon Electrodes. *Nat. Mater.* **2012**, *11*, 306–310.

(12) Breitsprecher, K.; Holm, C.; Kondrat, S. Charge Me Slowly, I Am in a Hurry: Optimizing Charge–Discharge Cycles in Nanoporous Supercapacitors. *ACS Nano* **2018**, *12*, 9733–9741.

(13) Li, Z.; Mendez-Morales, T.; Salanne, M. Computer Simulation Studies of Nanoporous Carbon-Based Electrochemical Capacitors. *Current Opinion in Electrochemistry* **2018**, *9*, 81–86.

(14) Jagiello, J.; Thommes, M. Comparison of DFT Characterization Methods Based on N2, Ar, CO2, and H2 Adsorption Applied to Carbons with Various Pore Size Distributions. *Carbon* **2004**, *42*, 1227–1232.

(15) Ravikovitch, P. I.; Neimark, A. V. Density Functional Theory Model of Adsorption on Amorphous and Microporous Silica Materials. *Langmuir* **2006**, *22*, 11171–11179.

(16) Toso, J. P.; Oliveira, J. C. A.; Maia, D. A. S.; Cornette, V.; López, R. H.; Azevedo, D. C. S.; Zgrablich, G. Effect of the Pore Geometry in the Characterization of the Pore Size Distribution of Activated Carbons. *Adsorption* **2013**, *19*, 601–609.

(17) Kupgan, G.; Liyana-Arachchi, T. P.; Colina, C. M. NLDFT Pore Size Distribution in Amorphous Microporous Materials. *Langmuir* **2017**, *33*, 11138–11145.

(18) Georgi, N.; Kolesnikov, A.; Uhlig, H.; Möllmer, J.; Rückriem, M.; Schreiber, A.; Adolphs, J.; Enke, D.; Gläser, R. Characterization of Porous Silica Materials With Water at Ambient Conditions. Calculating the Pore Size Distribution from the Excess Surface Work Disjoining Pressure Model. *Chem. Ing. Tech.* **2017**, *89*, 1679–1685.

(19) Nguyen, P. T.; Do, D.; Nicholson, D. Pore Connectivity and Hysteresis in Gas Adsorption: A Simple Three-Pore Model. *Colloids Surf. A* **2013**, *437*, 56–68.

(20) Chizmadjev, Y. .; Markin, V.; Tarasevich, M.; Chirkov, Y. *Macrokinetics of Processes in Porous Media*; Nauka, Moscow, 1971.

(21) Berk, N. F. Scattering Properties of a Model Bicontinuous Structure with a Well Defined Length Scale. *Phys. Rev. Lett.* **1987**, *58*, 2718–2721.

(22) Gommes, C. J.; Roberts, A. P. Structure Development of Resorcinol-Formaldehyde Gels: Microphase Separation or Colloid Aggregation. *Phys. Rev. E* **2008**, *77*, 041409.

(23) Prehal, C.; Koczwara, C.; Jäckel, N.; Schreiber, A.; Burian, M.; Amenitsch, H.; Hartmann, M. A.; Presser, V.; Paris, O. Quantification of Ion Confinement and Desolvation

in Nanoporous Carbon Supercapacitors with Modelling and in Situ X-Ray Scattering. *Nat. Energy* **2017**, *2*, 16215.

(24) Prehal, C.; Koczwara, C.; Jäckel, N.; Amenitsch, H.; Presser, V.; Paris, O. A Carbon Nanopore Model to Quantify Structure and Kinetics of Ion Electrosorption with in Situ Small-Angle X-Ray Scattering. *Phys. Chem. Chem. Phys.* **2017**, *19*, 15549–15561.

(25) Gelb, L. D.; Gubbins, K. E. Pore Size Distributions in Porous Glasses: a Computer Simulation Study. *Langmuir* **1999**, *15*, 305–308.

(26) Kondrat, S.; Georgi, N.; Fedorov, M. V.; Kornyshev, A. A. A Superionic State in Nano-Porous Double-Layer Capacitors: Insights from Monte Carlo Simulations. *Phys. Chem. Chem. Phys.* **2011**, *13*, 11359–11366.

(27) Lee, A. A.; Vella, D.; Goriely, A.; Kondrat, S. The Capacitance-Power-Hysteresis Trilemma in Nanoporous Supercapacitors. *Phys. Rev. X* **2016**, *6*, 021034.

(28) Kondrat, S.; Kornyshev, A. Pressing a Spring: What Does It Take to Maximize the Energy Storage in Nanoporous Supercapacitors? *Nanoscale Horiz.* **2016**, *1*, 45–52.

(29) Prehal, C.; Grätz, S.; Krüner, B.; Thommes, M.; Borchardt, L.; Presser, V.; Paris, O. Comparing Pore Structure Models of Nanoporous Carbons Obtained from Small Angle X-Ray Scattering and Gas Adsorption. *Carbon* **2019**, *152*, 416–423.

(30) Kondrat, S.; Kornyshev, A.; Stoeckli, F.; Centeno, T. The Effect of Dielectric Permittivity on the Capacitance of Nanoporous Electrodes. *Electrochem. Comm.* **2013**, *34*, 348–350.

(31) Weeks, J. D.; Chandler, D.; Andersen, H. C. Role of Repulsive Forces in Determining the Equilibrium Structure of Simple Liquids. *J Chem. Phys.* **1971**, *54*, 5237–5247.

(32) Widom, B. Some Topics in the Theory of Fluids. *J Chem. Phys.* **1963**, *39*, 2808–2812.

(33) Stauffer, D.; Aharony, A. *Introduction to Percolation Theory*; Taylor & Francis, 2014.

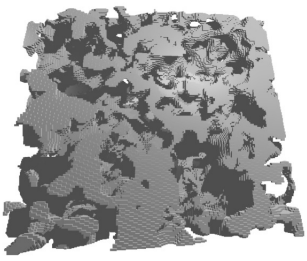

Activated-carbon
electrode